AGU ADVANCING EARTH AND SPACE SCIENCE

Water Resources Research

RESEARCH ARTICLE
10.1029/2021WR030426

Experimental Analysis of Mass Exchange Across a Heterogeneity Interface: Role of Counter-Current Transport and Non-Linear Diffusion

Monika S. Walczak[1], Hamidreza Erfani[1], Nikolaos K. Karadimitriou[2], Ioannis Zarikos[3], S. Majid Hassanizadeh[4], and Vahid Niasar[1]

[1]Department of Chemical Engineering and Analytical Science, University of Manchester, Manchester, UK, [2]Institute of Mechanics (CE), Stuttgart University, Stuttgart, Germany, [3]Environmental Research Laboratory, National Center for Scientific Research 'Demokritos', Agia Paraskevi, Greece, [4]Earth Sciences Department, Utrecht University, Utrecht, The Netherlands

Key Points:

- Mass exchange across a heterogeneity interface was quantified using optical imaging
- The linear mass exchange rate coefficient is non-unique and process-dependent
- Nonlinear diffusion and counter-current transport slow down the unloading process

Correspondence to:

V. Niasar,
vahid.niasar@manchester.ac.uk

Citation:

Walczak, M. S., Erfani, H., Karadimitriou, N. K., Zarikos, I., Hassanizadeh, S. M., & Niasar, V. (2022). Experimental analysis of mass exchange across a heterogeneity interface: Role of counter-current transport and non-linear diffusion. *Water Resources Research*, *58*, e2021WR030426. https://doi.org/10.1029/2021WR030426

Received 18 MAY 2021
Accepted 6 JUN 2022

Author Contributions:

Conceptualization: Vahid Niasar
Data curation: Monika S. Walczak, Vahid Niasar
Formal analysis: Monika S. Walczak, Hamidreza Erfani, Vahid Niasar
Funding acquisition: Vahid Niasar
Investigation: Monika S. Walczak, Hamidreza Erfani, Nikolaos K. Karadimitriou, Vahid Niasar
Methodology: Monika S. Walczak, Hamidreza Erfani, Nikolaos K. Karadimitriou, Ioannis Zarikos, S. Majid Hassanizadeh
Project Administration: Vahid Niasar
Resources: S. Majid Hassanizadeh, Vahid Niasar
Software: Monika S. Walczak, Vahid Niasar
Supervision: Vahid Niasar
Validation: Vahid Niasar

Abstract Solute transport in heterogeneous and fractured systems is a complex process given the permeability contrasts and the time scales discrepancies of transport in high-permeability versus low-permeability regions. We studied this phenomenon by injecting a solute (dyed water) in a micromodel comprising a single channel in contact with a porous medium and evaluated the mass exchange across the interface between the channel and porous medium (resembling the interface between free flow and porous media regions). Two sets of transport experiments were performed at three injection rates of 0.01, 0.1, and 1 ml/hr. Injection of dyed water into a clean-water-filled micromodel (referred to as the loading process hereafter) and injection of clean water into a dyed-water-filled micromodel (referred to as the unloading process hereafter). The dynamics of solute transport was recorded using time-lapse optical imaging. Our experimental results demonstrated the change of the mass exchange rate coefficient with time and a much smaller transfer rate coefficient during the unloading compared to the loading process. It is proposed that concentration-dependent counter-current advection-diffusion cause slow-down and further delay in the transport. These results may provide further explanation for the observed slow release of contamination in aquifers.

Plain Language Summary Solute transport in fractured aquifers is complex as the time scale of transport in fractures and matrix is very different. This study investigates how the mass exchange across a heterogeneity interface varies as a function of flow dynamics and the transport process. Detailed experimental analysis on a synthetic porous medium has been performed and the mass exchange has been quantified using the optical imaging of a tracer. Results can help better understanding the physics of the process and developing more physically based models which can assist the assessment of contaminant transport in fractured systems.

1. Introduction

Flow, transport, and mass exchange in heterogeneous porous media (e.g., high permeability-low permeability, fracture-matrix) can be found in many natural and industrial systems. Some examples are found in soil and groundwater remediation (Alfaro & Wong, 2001; Mutch et al., 1993; Paradis et al., 2018; Siegrist et al., 1999), enhanced oil recovery (Babadagli, 2003), radioactive waste management (De Windt et al., 1999; Suzuki et al., 2018), geothermal energy (Murphy et al., 1981; Shaik et al., 2011), restoration of subterranean aquifers (Masciopinto, 2006; Mutch et al., 1993), and drug delivery in medical science (Lima et al., 2008; Shaw et al., 2014).

Upscaling flow and transport in porous media with heterogeneity interfaces (i.e., abrupt change of porosity and permeability) is challenging and complex as transport time scales in both domains are significantly different due to their permeability contrast. The sharpest permeability contrast can be found in fracture-matrix systems as flow in fractures and porous media can be described by Navier-Stokes (or Stokes) equation and Darcy's law, respectively. While transport in fractures can be advection dominated, transport in matrix has been usually assumed to be diffusive. Significant efforts have been made to describe the interface conditions between a fracture and a matrix to guarantee the mass, momentum, and energy balance across the interface (Berkowitz, 2002; Jamet et al., 2009; Layton et al., 2002; Mosthaf et al., 2011; Ochoa-Tapia & Whitaker, 1995). Momentum conservation is a common

Visualization: Monika S. Walczak, Hamidreza Erfani, Vahid Niasar
Writing – original draft: Monika S. Walczak, Hamidreza Erfani, Vahid Niasar
Writing – review & editing: Monika S. Walczak, Hamidreza Erfani, Nikolaos K. Karadimitriou, Ioannis Zarikos, S. Majid Hassanizadeh, Vahid Niasar

approach for interface coupling (Layton et al., 2002), however, this condition does not hold when the average pore velocities vary significantly between the domains (Hasan et al., 2019; Saffman, 1971). Another widely used boundary condition is the slip velocity condition on the interface, introduced by Beavers & Joseph (1967). Recently, Weishaupt et al. (2019) introduced a novel monolithic numerical approach based on mechanical equilibrium in order to couple free flow (Stokes flow) and pore-network model (using Hagen-Poiseuille flow) at pore scale to illustrate the impact of pore network structure (structured or unstructured networks) as well as pore size on the solute transport.

In several Darcy-scale studies, the solute transport in the fracture was assumed to be purely advective and solute transport in the matrix to be purely diffusive (Bodin et al., 2003; Roubinet et al., 2012; Ohlsson & Neretnieks, 1995). Based on similar assumptions, analytical solutions for a single fracture connected to a semi-infinite matrix were developed (Tang et al., 1981). Further analytical solutions considered various fracture-matrix configurations to represent natural systems more realistically (Sudicky & Frind, 1982; West et al., 2004). It was shown that the ratio of transversal dispersion flux in the fracture to the longitudinal diffusion flux in the matrix is the main controlling factor of the fracture-matrix mass exchange rate (Falta & Wang, 2017; Houseworth et al., 2013; Roubinet et al., 2012). These studies assumed the interface coupling condition, the advective mass exchange across the interface and the dispersion in the matrix due to flow in the channel were negligible. Due to the significant difference between transport time scales in fractures versus the matrix, the temporal evolution of mass transfer in the whole system cannot be quantified by a single velocity and a constant dispersion coefficient. This scale-dependent transport behavior is often referred to as "non-Fickian" or "anomalous" (Berkowitz, 2002). Non-Fickian transport has also been observed in homogeneous unsaturated (Aziz et al., 2018; Bromly & Hinz, 2004; Hasan et al., 2019, 2020; Karadimitriou et al., 2016; Padilla et al., 1999; Sharma et al., 2016) as well as single-phase heterogeneous porous media (An et al., 2020; Berkowitz & Scher, 2009; de Vries et al., 2017; Le Borgne & Gouze, 2008; Roubinet et al., 2013) and at field-scale (Berkowitz, 2002; Cortis et al., 2004).

Commonly used continuum-scale approaches to model solute transport in fractured porous media is to use the double (or multi-) porosity and double (or multi-) permeability schemes (Dejam et al., 2014; Di Donato & Blunt, 2004; Douglas Jr & Arbogast, 1990; Haddad et al., 2012). In these models, the whole system is idealized to be a uniform, well-connected network of flow channels and a stack of matrix blocks. The common assumption in such models is that the regions occupied by the fluid can be classified to mobile (flowing) and immobile (stagnant) regions. The interface between these two regions is assumed to be controlled by a simple single rate physical non-equilibrium mass transfer (De Smedt & Wierenga, 1979) or a multi-rate non-equilibrium mass transfer (Haggerty et al., 2004), relating the average concentration difference between fracture and matrix. Alternatively, the continuous time random walk (CTRW) model (Berkowitz et al., 2006), which is a stochastic approach employing different probability density functions for various domains, can be used. Ling et al. (2016) used perturbation theory to study solute transport in a coupled fracture-matrix system. They concluded that the effect of matrix properties on the macroscopic dispersion coefficient was controlled by the magnitude of Péclet number (*Pe*, is defined as the ratio of the advective to diffusive transport). Depending on the Péclet number, they characterized the fracture-matrix solute transport to three regions of diffusion dominant, transition, and advection-dominant. It was shown that at small Péclet numbers the dispersion coefficient is independent of both matrix permeability and flow rate, while for high Péclet numbers (advection dominated) the flow rate and the matrix permeability become important.

To evaluate pore-scale flow and transport physical processes in a fracture-matrix system, micro-scale experimental research has been used. The model of Ling et al. (2016) presented simulation results of permeable obstructions with periodic structures assuming advective transport from fracture to matrix. In another study, Polak et al. (2003) used X-ray imaging to study NaCl diffusion into an artificially fractured chalk core. They studied both injection and clean-up of NaCl scenarios. Based on experimental results and measured concentration fields, they concluded that the clean-up process needs a much longer time, compared to injection of NaCl. The same visualization methodology was used at the core-scale by other researchers and similar conclusions were made (Alajmi et al., 2009; Zhu et al., 2007). Other experimental studies related to fracture-matrix transport focused on validating the continuum-scale models (Ling et al., 2018), the contribution of both diffusion and advection mechanisms (Wan et al., 1996), and estimation of the velocity field (Ahkami et al., 2019).

The present study extends the understanding of transport across the heterogeneity interface. Using a channel-porous media micromodel following objectives have been sought: impact of flow rate in the channel

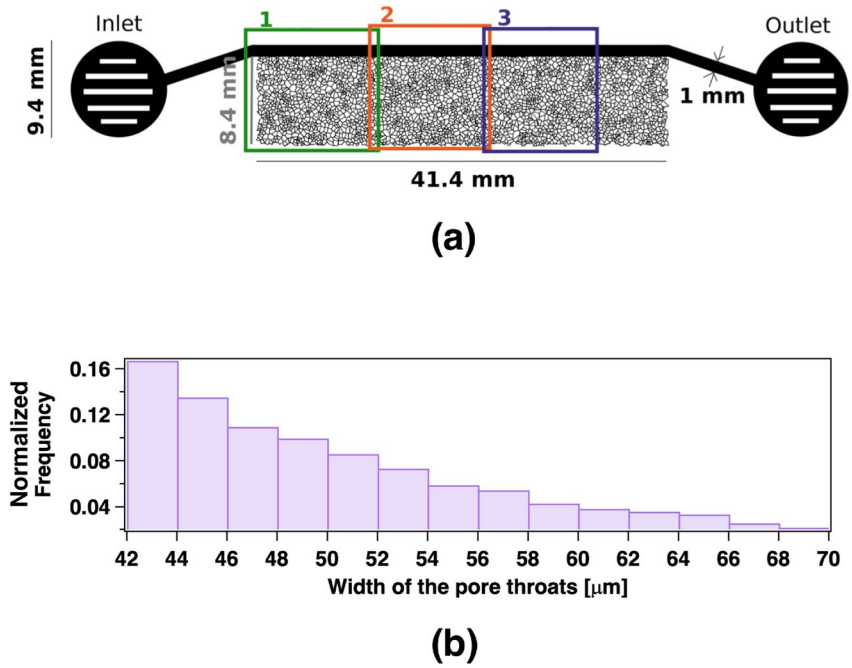

Figure 1. (a) Planar view and geometry of the channel-porous medium micromodel with marked boxes, illustrating the visualized windows using three digital cameras. The inlet and outlet areas were locally perforated in order to inject/extract the liquid. (b) Distribution of the normalized frequency of pore widths, which are in average 20 times narrower than the channel.

on the mass exchange rate coefficient for a linear non-equilibrium mass exchange, impact of transport process (injection or removal of concentration) on the mass exchange rate coefficient, and spatial variability of transport regime in the porous medium. Unlike former experimental studies, our work provides detailed pore-scale images of the spatial distribution of ink (i.e., tracer) to quantify the mass exchange rate under different flow conditions during both loading and unloading experiments. Anomalies observed during the unloading process are discussed and a simple model is developed to explain the observations. This manuscript in organized as follows: after introducing the materials and methods, experimental procedure and image analysis are explained. Results related to the concentration profiles in the porous medium and channel sections, mass exchange between the porous medium and the channel, and the mass exchange rate coefficients and discussions are presented. Finally, the key conclusions and potential implications for the large-scale modeling works are discussed.

2. Materials and Methods

2.1. Micromodel Design and Fabrication

The micromodel was made of Poly-Di-Methyl-Siloxane (PDMS) and the pattern comprised a single channel connected to a porous medium (Figure 1a). The negative pore space pattern was imprinted on a silicon wafer by standard photolithography, which was used as a mold (Karadimitriou & Hassanizadeh, 2012). The PDMS material, filling the patterns on the silicon wafer, created the solid domain of the micromodel. This was fused to another PDMS slab to manufacture a percolating network of pores with constant depth and variable planar width. The structure of the porous medium was generated based on Voronoi diagram, which has the structure and connectivity of a generic porous medium (Ghassemzadeh et al., 2000; Wu et al., 2012). The distribution of pores width are shown in Figure 1b varied between 42 and 70 μm. The depth of the micromodel was 57 μm and the overall porosity of the porous medium was 0.33. The porous medium was 41.4 mm long and 8.4 mm wide. The channel was 1 mm wide. Given the constant depth for the channel and the porous medium and considering the reported channel width and average pore width, the permeability for the channel and porous medium were estimated to be 260 and 99 μm^2, respectively.

2.2. Experimental Setup

The micromodel was horizontally positioned under a collimated LED light source for a uniform illumination over the micromodel. Subsequent to passing through the micromodel, the beam of light was redirected via a 50 × 50 mm prism (Edmund Optics) into a magnifying lens (SONY Sonnar, f 1.8/135 mm). A set of three beam splitters (Edmund Optics) were positioned behind the magnifying lens, splitting the light into four identical beams, each being detected by a 5-Megapixel digital camera (Prosilica GC-2450). Given the relative position of the optical elements, one pixel of the captured image corresponding to a 5.4 × 5.4 μm area of the micromodel. A more detailed description of the experimental setup can be found elsewhere in former studies (Karadimitriou, 2013; Karadimitriou et al., 2012). The solute transport was studied by either injecting dyed water into the clean water-saturated micromodel (loading) or by injecting clean water into the dyed water-saturated micromodel (unloading). Three different flow rates, namely 0.01, 0.1, and 1 ml/hr of dyed water or clean water were injected using a syringe pump (Pump 11, Pico Plus Elite, Harvard Apparatus). The Reynolds number, calculated for the fastest flow rate in an enclosed tube of the same hydraulic diameter as the channel was 0.52. Reynolds number smaller than 1 indicates that the fluid flow inside the micromodel structure was laminar (Bear, 2013). A set of monochrome images were acquired using a fixed time interval for each flow rate during the loading and unloading experiments. Three cameras captured the partial length of the channel-porous medium system, as shown with marked boxes in Figure 1a. Note these boxes are larger than the representative elementary volume (REV) and averaged concentration in each box presents a Darcy-scale concentration.

2.3. Image Processing and Data Analysis

The resident solute concentration was calculated for the channel and the porous medium, separately. The intensity scale was inverted such that a pixel corresponding to the higher concentration of the solute was represented by a higher intensity value compared to a pixel in the clean water domain. For calculation of concentration from the gray-scale intensities, we performed a correlation between the measured concentrations and the gray-scale intensities, which showed an exponential trend. Denoting a global maximum, $I_{\max}$, and minimum intensity, $I_{\min}$ for a pixel throughout the sequence of images, the normalized intensity and the calibrated concentration for pixel i was determined by $I_i' = (I_i - I_{\min}) / (I_{\max} - I_{\min})$ and $C_i = a\left(1 - e^{bI_i'}\right)$, respectively. a and b are calibration coefficients. Subsequently, the normalized average concentration of the solute in a region of Γ covering n_Γ number of pixels is given by $C_\Gamma = \frac{1}{n_\Gamma} \sum_{i \in \Gamma} C_i$, where Γ denotes the channel (f) or porous media (m) domains. Commonly, the mass exchange between the channel and porous medium has been proposed to be proportional to the concentration difference between the domains (Haggerty et al., 2004). So, the mass exchange rate coefficient versus time was defined as follows:

$$\alpha(t) = \frac{\partial_t C_m}{C_f(t) - C_m(t)} \tag{1}$$

3. Results and Discussion

3.1. Channel-Porous Medium Interface Condition

The mass and momentum transfer across low and high permeability regions is significantly controlled by the permeability contrast and viscous stress at the interface. As shown in Figure 2a, the velocity profile in the channel does not follow a symmetric parabolic profile due to different side boundaries. While the top boundary of the channel is closed and can be assumed to be a no-slip boundary, the lower boundary is leaky. Thus, an asymmetric velocity profile is expected. This has been demonstrated by early time imaging of the concentration front in the channel. Using the acquired images during the experiments, deviation of the extremum of the solute concentration profile from the center of the channel was estimated as shown in Figure 2a. Since we could not measure the velocities at the interface between the channel and porous medium (that would require access to microPIV equipment), the deviation of the extremum will be a proxy of the slip condition. We defined the asymmetry factor as $AS(x, t) = (H - H^*(x, t))/H$, which can change between −1 and 1. H denotes the half-width of the channel, and $H^*(x, t)$ denotes the distance between the leaky interface and the position of the extremum of the concentration front. Given the steady-state flow in the channel, we safely assumed that $AS(x, t) = AS(x)$. $AS(x) = -1$ indicates that the concentration extremum is positioned at the non-permeable wall of the channel, and for $AS(x) = 1$, the

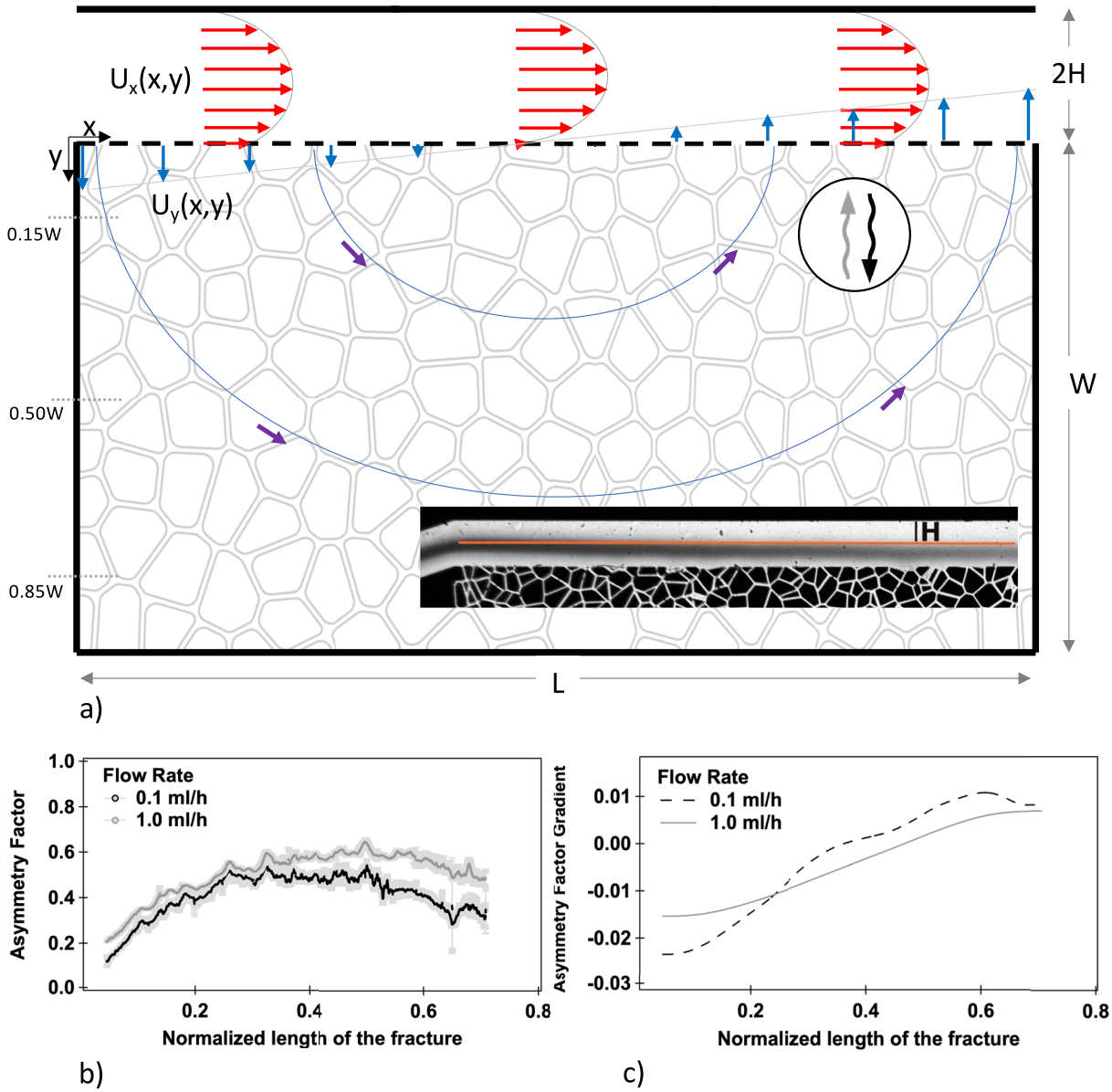

Figure 2. The channel-porous medium interface condition. (a) schematic presentation of velocity profile in the channel and streamlines in the porous medium, inset: Deviation of the extremum of the front solute concentration profile from the center of channel, due to the permeable interface between the channel and the porous medium. The black and gray wavy arrows inside the circle indicate the general direction of diffusion during loading and unloading, respectively (b) The asymmetry factor along the channel at flow rates of 0.1 and 1 ml/hr and (c) gradient of the asymmetry factor along the channel.

extremum of the concentration reaches the leaky interface. Variations of the asymmetry factor along the channel for two rates of 0.1 and 1 ml/hr are shown in Figure 2b.

At the inlet of the channel, $AS(0)$ is almost zero, which indicates the symmetric velocity profile at the inlet. However, close to the half-length of the channel, the asymmetry factor increases to 0.5–0.6 and then decreases along the second half of the length as explored below. Moreover, the trends of the asymmetry factor were fairly similar for both injection flow rates. Considering the variation of the asymmetry factor along the channel (Figure 2c), we can speculate that the normal component of velocity (u_y) at the interface is at maximum (normal toward the porous medium interface) just after the inlet ($\partial_x AS$ is negative). In the half-length distance, $\partial_x AS \approx 0$, which indicates $u_y \approx 0$. After the half-length distance, again the magnitude of u_y increases but with a direction toward the channel. With increase of the injection rate in the channel, the normal velocity (as well as the slip velocity) increased, as expected. Similar results were reported computationally in the recent work of Weishaupt

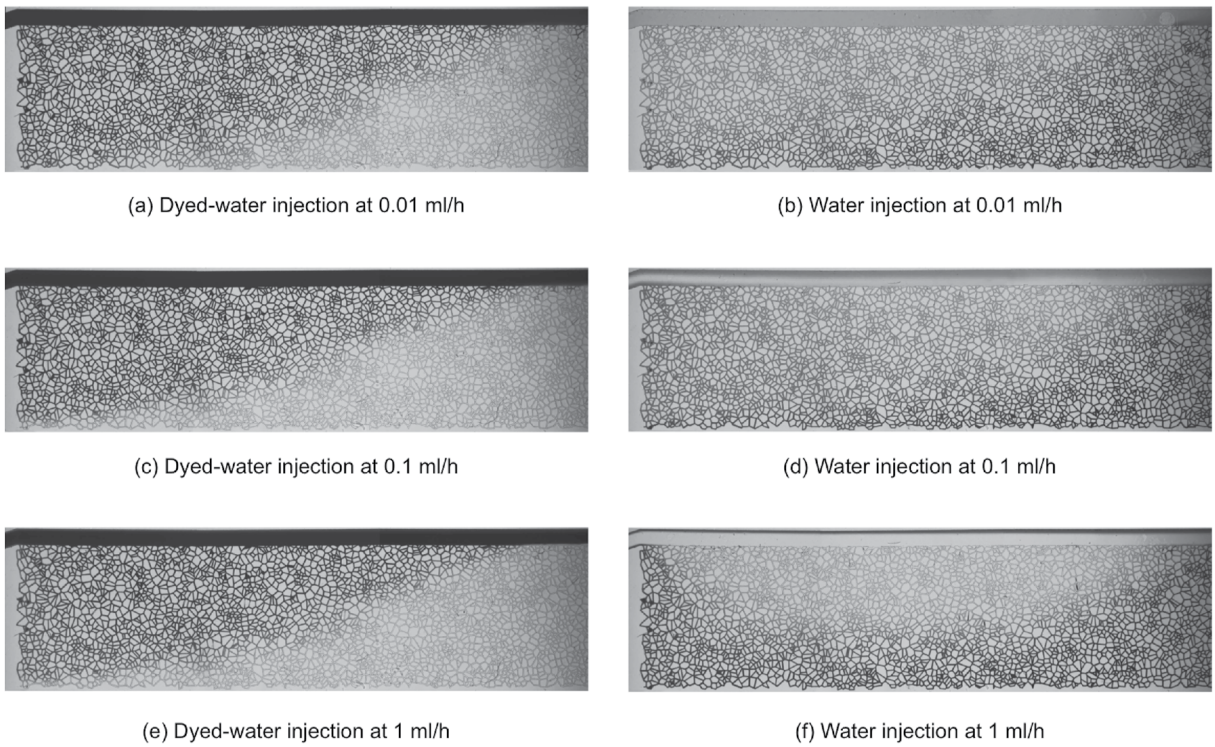

Figure 3. Snapshots of the concentration field in the channel and porous medium during dyed-water injection (loading) and clean water injection (unloading) at injection rates of 0.01, 0.1, and 1 ml/hr. The field of view shows stitched images taken by 3 cameras at the same time. Average concentration in the porous medium in all images is 0.5.

et al. (2019), who combined Stokes flow and pore-network modeling. These results clearly show the mass and momentum exchange between the channel and porous medium control the solute transport in the porous medium. As expected, the injected fluid initially mixes with and displaces the fluid in the channel due to the larger hydraulic permeability of the channel compared to the porous medium. However, due to the structure of channel-porous medium interface and resulting transverse velocity, the boundary conditions play a role in the solute transport into/out of the porous medium. This will be further discussed by looking at the concentration profile in the porous medium.

3.2. Resident Concentration Profiles in the Porous Media and the Channel

The resident concentration front shapes are distinctly different during loading and unloading processes, as depicted in Figure 3 for an average resident concentration of 0.5 in the porous medium. The experimental constraints did not allow to record images near the injection point. However, the consistency of spatial concentration pattern in fracture for numerous repetition of experiment excludes the presence of randomly positioned residues of ink and reported concentration maps are not due to ill-defined or uncontrolled injection effect.

For the case of loading, the advective transport flux ($J = cv$) is normal toward the porous domain in the left half of the system (upstream) and is outwards the porous medium in the right half of the system (downstream). v stands for the pore velocity. In the case of diffusive transport flux $J = -D\nabla c$ (D stands for the the hydrodynamic dispersion which is the summation of mechanical dispersion and diffusion), it is always toward the porous medium in the case of loading and it is outwards the porous medium in the case of unloading as the the resident time in the channel is much smaller than that of the porous medium. As a result, during the loading in the left half of the system, the advective and diffusive fluxes are co-current and in the right half of the system, they are counter-current. For the case of unloading processes, the advective and diffusive fluxes are counter-current in the left half and they are co-current in the right half of the domain. Therefore, significantly different concentration fields have been developed for the loading and unloading processes. Also, since the advective transport highly depends on the injection rate, the spatial concentration field during the unloading process at higher flow rates,

namely 0.1 and 1 ml/hr portrayed larger solute concentration close to the left boundary of the porous domain compared to the center of the field (Figures 3d and 3f). These results are in agreement with the schematic streamline presentation in Figure 2a.

Notably, there is an effect of the flow rate as well as the porous medium boundary on the concentration fronts. At the slowest injection rate for the unloading process (i.e., 0.01 ml/hr water injection), the effect of the closed boundaries of the porous domain (left, right, and bottom sides) is not significant, Figure 3b. However, with an increase of the flow rate (i.e., 0.1 and 1 ml/hr water injection) the impact of the closed boundaries becomes significant, Figures 3d and 3f. Results clearly show that the longitudinal and lateral dispersion components are significantly different at high injection rates. This behavior is less visible in the former micromodel study of Ling et al. (2018), where a high porosity and very regular solid space with smooth round boundaries was used. However, unlike our system, the channel-porous medium mass exchange rate was fully controlled by diffusion. Also, the impact of shear velocity on the transport was fully ignored in their proposed analytical solutions.

The multi-modal behavior (Siirila-Woodburn et al., 2015) of the resident concentration curve in the present study is presented in Figure 4. This clearly indicates that there are regions of contrasting flow velocity in the channel-porous medium system due to transverse dispersion, which strongly change with the position with respect to the heterogeneity interface. The multi-modal behavior also strongly change with the process as they are visible in the unloading process, while in the loading process, the concentration profiles are still Fickian. To address the effect of lateral dispersion on change of resident concentrations, a simple model has been proposed which will be discussed in the next section.

The temporal change of resident concentrations for each window and the total field of view are shown in Figure 5. The concentration calculations were done separately for the channel and the porous domain. Note that the left column is associated with the loading case and the middle column is associated with the unloading case and the right column shows the mass-exchange rate coefficient for loading and unloading with time. The presented resident concentration curves for the loading process follow closely the so-called S-shape behavior observed in Fickian transport (Berkowitz, 2002). However, during the unloading process, the resulting curves do not follow the classical Fickian transport profiles. There is a slow-down period in the curves (Figures 5e and 5h), at which the change of concentration in the porous medium does not follow the Fickian profile.

This behavior is more significant at high injection rates during the unloading process due to the significant difference between the advective and diffusive time scales. The slow-down period starts at 1,050, 1,230, and 1,500 s for windows 1 to 3, respectively for the injection rate of 0.1 ml/hr (Figure 5e). These times correspond to injected pore volumes (PV, defined as the volume of the void space in the channel and porous domain in one window) of 9.2, 9.9, and 11.2, respectively. Similarly, for the injection rate of 1 ml/hr in Figure 5h, the slow-down period starts at 130, 160, and 190 s for windows 1 to 3, respectively, corresponding to 12.3, 12.7, and 13.4 PV, respectively.

3.3. Mass Exchange Across the Heterogeneity Interface

While the injection rates for the loading and unloading processes are identical, the slow-down period was only observed in the two higher rates during the unloading as shown in Figures 4 and 5. This behavior implies the importance of counter-current mass flux during the unloading. While advective transport is from the channel toward the porous domain, the mass transport by diffusion, or chemical potential difference, is from the concentrated regions in the porous domain toward the channel. Therefore, at the slow-down period, it seems that the magnitudes of these two transport mechanisms are more or less similar. In the channel, a similar behavior was also observed. The concentration profiles in the channel indicate the slow-down period around 700–1,100 s for the flow rate of 0.1 ml/hr, and 90–160 s for 1 ml/hr. The values do not vary between different windows due to the high velocities in the channel. Such slow-down periods were not observed during the loading process as advection and diffusion were both mainly acting in the same direction.

The mass exchange rate coefficient (α using the linear non-equilibrium model in Equation 1) versus time for both unloading and loading processes are shown in Figures 5c, 5f and 5i. varies significantly (3–4 orders of magnitude) with time, which highlights how inaccurate the concept of a constant mass exchange rate coefficient is. Similar results for variable mass exchange rate coefficients were reported by Hasan et al. (2019) and

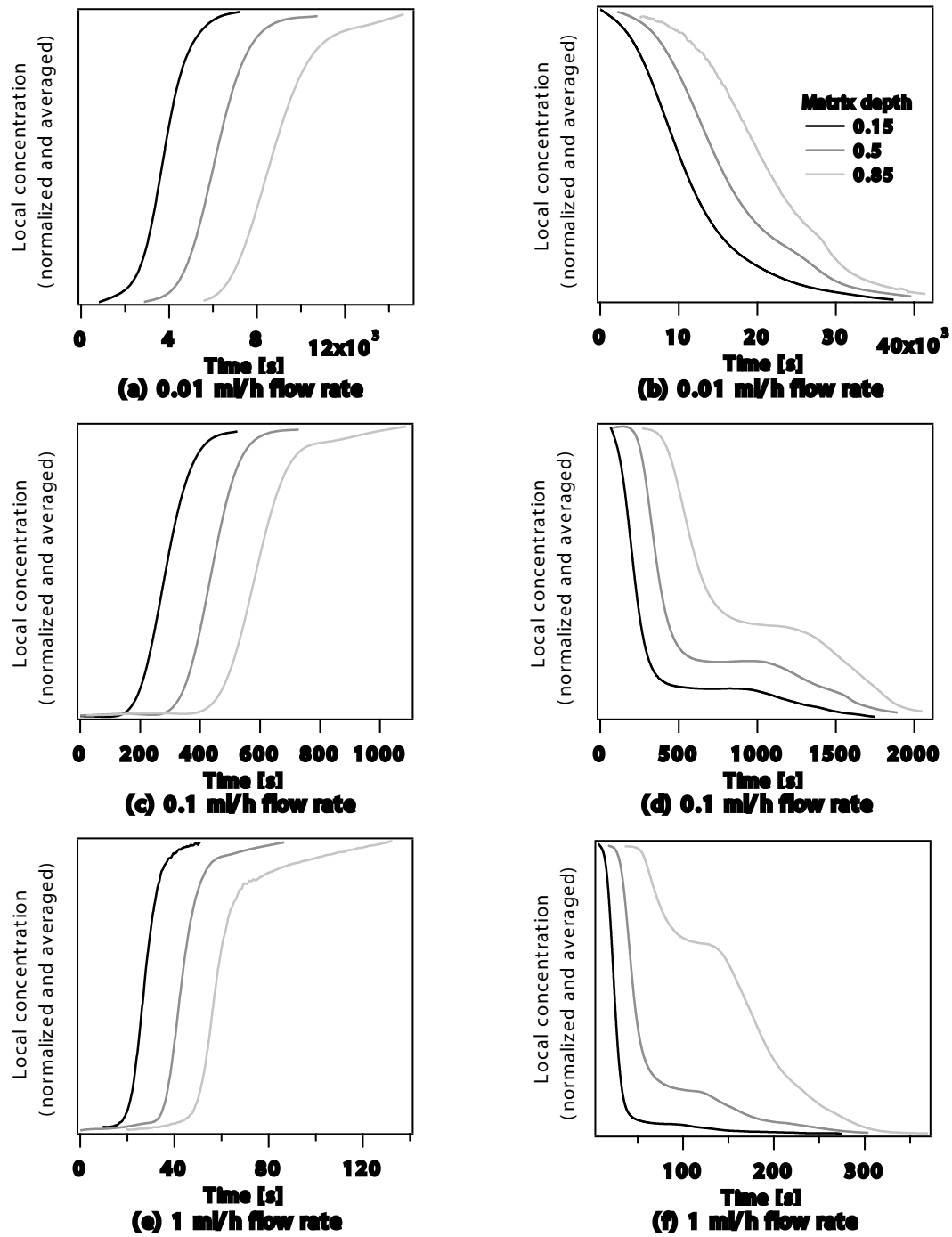

Figure 4. Local concentration curve averaged over the length of the porous medium at difference distances of 0.15, 0.5, and 0.85 of porous medium width (respect to the heterogeneity interface, see Figure 2). Concentration changes are presented for the loading and unloading at three flow rates of 0.01, 0.1, and 1 ml/hr.

Karadimitriou et al. (2016). The right column of Figure 5 illustrates the non-uniqueness of the mass exchange rate coefficients, which vary strongly with the injection flow rate.

During the unloading process, the mass exchange rate coefficient (α) exhibits oscillatory behavior for all windows at 0.1 and 1 ml/hr flow rates. We speculate that the oscillatory behavior is due to the multi-directional dispersion in the porous medium. As a result, the scalar mass exchange rate coefficient cannot correctly capture the dynamics of the mass exchange, which is controlled by the tensorial nature of the transport in the channel and

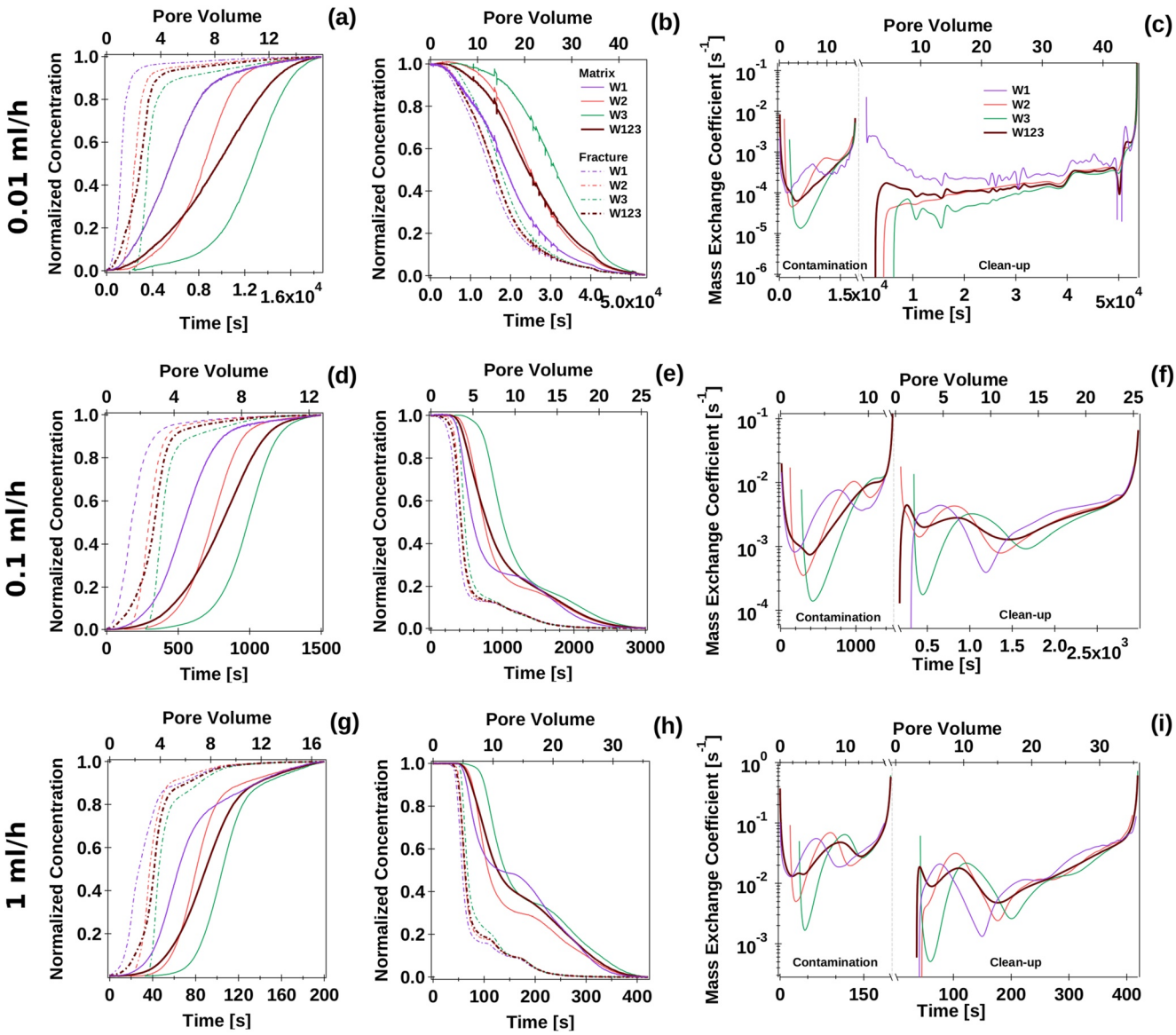

Figure 5. (a and b, d and e, g and h) Normalized solute concentration as a function of time during the injection of dyed water/clean water at flow rates of 0.01, 0.1, and 1.0 ml/hr. Concentration profiles were calculated for the channel and porous domains in each imaged window, separately. The overall resident concentration from the combined field of views are also presented. (c,f,i) Mass exchange rate coefficient during the loading and unloading as a function of time at three different flow rates.

porous domain. Such oscillations in the mass exchange rate coefficient confirm the complex character of mass exchange across heterogeneity interfaces. Besides porous media characteristics such as pore morphology and permeability tensor, the mass exchange is strongly dependent on the Péclet number variation across the interface (Ling et al., 2018). In summary, based on the provided experimental results, the behavior of the mass exchange rate coefficient is similar for all windows at the same flow rate, while the pattern seems to change as a function of the injection flow rate. This implies that α is highly sensitive to the flow rate and the hydrodynamic conditions between the two domains. Note that due to the differences in the boundary conditions of the windows, the mass exchange rate coefficients are not identical for all of them. Given the flow direction from left to right, the left boundary of the window three is open, in contrast to the window 1, where the left boundary is closed. The extremum of mass exchange rate coefficient for the flow rates of 0.1 and 1 ml/hr (Figures 5f and 5i) for the unloading part appear to correspond to the slow-down period (Figures 5e and 5h).

To explicitly show the dependence of the mass exchange rate coefficient on the hydrodynamics in the channel, time-averaged mass exchange rate coefficient was calculated as a function of the injection rate for both loading

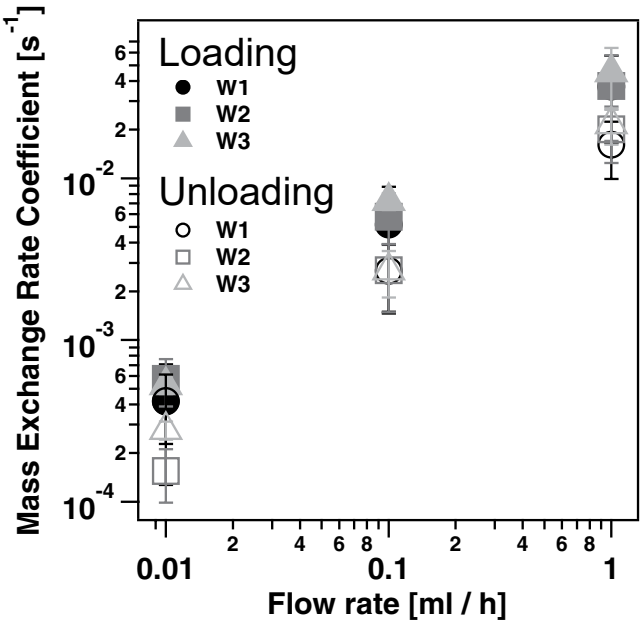

Figure 6. Time-averaged mass exchange rate coefficient as a function of injection rate in the channel. The error bars are referring to the Q50 of variation of α over the time period. During the loading the mass exchange rate is larger than that during the unloading.

and unloading processes for all windows, as shown in Figure 6. The mass exchange rate coefficient increases with an increase of the injection rate, which highlights the shortcomings in the theoretical and modeling developments, where the hydrodynamic dependence of the mass exchange rate coefficient is ignored. Also, the mass exchange rate coefficient during the loading is larger than unloading. This implies the impact of counter-current transport mechanisms (advection vs. diffusion), resulting in smaller mass exchange rate coefficients. The error bars show the Q50 (median) variation of the mass exchange rate coefficients during the averaging time period.

Comparison between experimentally obtained and theoretically predicted mass transfer coefficients poses a few challenges when the inverse analysis (fitting of the breakthrough curve) by means of integro-differential approach is being employed. The multi-modal predictions/methodology most often rely on a single-pulse injection signal (Boon et al., 2017; Moreno & Tsang, 1991). Some models do not allow the mass exchange between the transport channels (Maloszewski et al., 2005) or the number of considered channels are reduced to channel and porous medium only (Moreno & Tsang, 1991). In our study, the solute inflow was continuous compared to the time of the experiment, and mass transfer took place over the entire length of the heterogeneity interface; given the observed slipped velocity phenomena and likely there were separate flow pathways in porous domain (note the appearance of local peaks in Figures 4d and 4f and Figures 5e and 5h). Multi-rate mass transfer models commonly employ the analytical formula for the memory function (Wang et al., 2005). However, at least two distinct slopes are distinguishable (Figure 4), and thus likely distinct formulas for memory function should be applied (Haggerty et al., 2000). The breakthrough curve de-convolution is necessary before the application of any multi-rate model like multi-rate mass transfer, CTRW, or fractional advection-dispersion. This is explored in the next section provided in the following section. An interesting interpretation of anomalous transport in heterogeneous or fractured porous domain has been proposed by Edery et al. (2016) where the role of transverse transport/flow is emphasized. Given the geometry of the induced flow pathways in the porous domain, this could be likely a factor of the anomalous behavior of transport in the discussed micromodel, which has been discussed in the next section.

Given that the viscosities of dyed water and clean water are similar and non-Fickian behavior is only visible during the unloading process, there should be a nonlinearity in advection versus diffusion. To be specific, the advection and diffusion act in the same direction during the loading process. However, given that diffusion is governed by the chemical potential gradient, it acts in the opposite direction of advection during unloading. A potential reason for this non-linearity might be the non-linear diffusion (concentration dependent diffusion coefficient) which has been formerly addressed in the literature Carey et al. (1995); Dunlop & Stokes (1951); Harned and Nuttall (1949); Matuura and Koga (1959); McCall and Douglass (1965). In the following section, we aim to test the effect of both counter-current transport fluxes as well as the non-linear diffusion on the evolution of the resident concentration field.

4. Modeling-Assisted Interpretation of Results

As discussed earlier, examining the experimental data in Figure 4, the following key observations can be made: Observation (1) At a given injection rate, all the unloading experiments demonstrated longer time scale compared to the loading ones. Observation (2) Only during unloading experiments, local concentration ($\partial_t C = 0$) remained constant for a period of time, referred to as the slow-down period. The farther from the channel-porous medium interface, the slow-down period happens at smaller concentrations.

To capture these two key observations we propose a simple one-dimensional model, resembling the path flowing a streamline in the porous medium Section 2. Note the velocity field and concentration transport field are two-dimensional and reducing one dimension imposes significant simplifications as the boundary conditions of

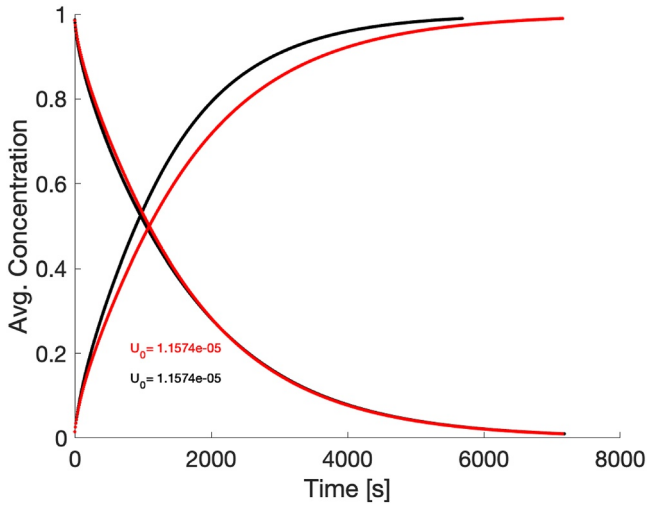

Figure 7. Average normalized concentration in a 1D model for a constant (red) and concentration-dependent (black) diffusion coefficient for both loading and unloading processes for the following conditions $v = 1.15 \times 10^{-5}$ m/s, $\beta = 2$, $\gamma = 3$, $L = 0.04$ m, $\alpha_d = 2$ mm, $D_m = 10^{-8}$ m^2/s. Constant inlet boundry and $\partial_x C = 0$ for outlet boundary were assigned.

the 1D domain is controlled by the 2D nature of transport. One-dimensional advection-dispersion is solved

$$\partial_t C = -\partial_x (vC - D\partial_x C) \tag{2}$$

D denotes the hydrodynamic dispersion, which is the summation of mechanical dispersion and molecular diffusion: $D = D_h + D_m$. As hydrodynamic dispersion can be presented as $D_h = \alpha_d v$, in which α denotes the dispersivity, then we can write:

$$D = \alpha_d v + D_m \tag{3}$$

Please note the molecular diffusion and effective diffusion in porous media will be different. To test the hypothesis whether with a constant effective diffusion coefficient, unloading will be slower than the loading experiments, we simulated experiments with constant concentration at the inlet and no dispersion of concentration ($\partial_x C = 0$) at the outlet. Figure 7 show that regardless of flow rate for advective or diffusion regime, the transport time scales are identical for the loading and unloading conditions. Thus, it can be concluded that either advective forces or diffusion forces need to behave differently for the loading or unloading processes. Recently Erfani et al. (2021); Y. Chen et al. (2021); Z. Chen et al. (2022) have also reported a larger time scale for unloading versus loading. Based on the the former studies which reported concentration-dependent diffusion coefficient (Carey et al., 1995; Dunlop & Stokes, 1951; Harned & Nuttall, 1949; Matuura & Koga, 1959; McCall & Douglass, 1965), we have proposed an empirical function for the diffusion coefficient as follows:

$$D_m = D_m^0 (1 + \beta C^\gamma) \tag{4}$$

For the same flow velocity and other system parameters but β and γ equal to 2 and 3, respectively, it is clear that loading process is faster than the unloading one.

This conceptual results show that although the counter-current fluxes happen for the unloading process, they are not responsible for the difference in the time scale of processes and the nonlinearity in the diffusion (or any other nonlinearity in advection vs. diffusion) is responsible for the difference in the time scales.

Regarding the observation 2 which indicates $\partial_t C = 0$, as explained earlier due to the counter-current advection versus dispersion during the unloading, these two fluxes may cancel out each other for a period of time. We conjecture that the outflow concentration of the model should be time-variable as the concentration field is two-dimensional, given the importance of the lateral dispersion and the two-dimensional transport field. Thus, we propose the outlet concentration as follows:

$$C_{out} = \begin{cases} 0.5\left[\operatorname{erfc}\left(\dfrac{L - v(t - t_c)}{2\sqrt{Dt}}\right) + \exp(Lv/D)\operatorname{erfc}\left(\dfrac{L + v(t - t_c)}{2\sqrt{Dt}}\right)\right), & \text{for loading} \\ 1 - 0.5\left[\operatorname{erfc}\left(\dfrac{L - v(t - t_c)}{2\sqrt{Dt}}\right) + \exp(Lv/D)\operatorname{erfc}\left(\dfrac{L + v(t - t_c)}{2\sqrt{Dt}}\right)\right), & \text{for unloading} \end{cases} \tag{5}$$

t_c indicates the time at which the outlet concentration starts to change, which is due to the different velocity magnitudes in the porous medium depending on their distance to the interface with the channel. Please note the exact time of that is not known given the two-dimensionality of the porous medium. As a result of concentration-dependent diffusion coefficient and time-variable outlet concentration, loading and unloading curves at different velocities have been simulated and shown in Figure 8. The velocity magnitude will decrease with distance from the interface.

The trends of the curves are very much similar to the experiments reported in Figure 4 and clearly similar to the experiments, the slow-down periods are only visible during the unloading process. With the increase of velocity,

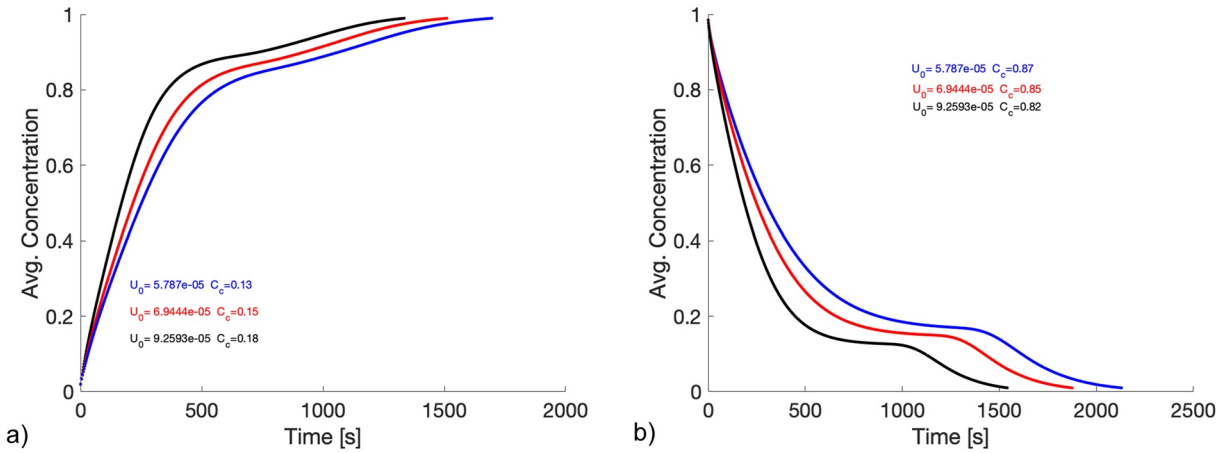

Figure 8. Average normalized concentration in a 1D model for a concentration-dependent diffusion coefficient and time-variable outlet concentration as a result of Equation 5.

slow-down period happens at lower concentrations since the counter-current diffusion would hinder transport. Although the provided analysis justifies the hypothesis of this research, the proposed model can be further developed to a bundle of parallel 1D domains (similar to a bundle of tubes) at difference length and velocities to mimic the whole domain and by integration over the whole 1D systems, the residence concentration of the whole porous medium can be simulated. Finally, we would like to emphasize that these learning of these experimental results and the model can play a significant role in understanding and modeling of large-scale transport problems. In subsurface applications such as nitrate contamination (Wang et al., 2016) a very long lag time has been observed between the nitrate contamination (loading) and time scale of nitrate release in the subsurface (unloading). The findings of this study may provide further explanations to this huge lag time, especially give the small advective forces in the subsurface.

5. Conclusions

Heterogeneity interface introduces major complexity due to mass and momentum exchange at the interface. Additionally, the complex nature of dispersion (its tensorial behavior and dependence on flow conditions) and upscaling transport as well as mass exchange across the heterogeneity interface is very challenging. In the present study, we designed and fabricated a micromodel comprising a single channel in contact with a rectangular porous domain, which is closed from other three sides. Using optical imaging, the resident concentration in the channel and porous domain at three different injection rates were characterized and the mass exchange rate across the interface - as a Darcy-scale entity - were quantified.

Results indicate that at heterogeneous porous media, given the tensorial behavior of dispersion, mass exchange cannot be simply captured by a constant scalar value and a robust physical-based mass exchange relation is missing. Moreover, our experimental observations showed that change of resident concentration with time during loading and clean up were fundamentally different. The resident concentration profiles during the loading were Fickian at different rates, while they were strikingly non-Fickian during the unloading, especially at higher injection rates. Note the porous medium and hydrodynamic conditions were identical. These observations open new questions to identify the physical reasons behind the asymmetric transport behavior during loading and unloading. One potential reason can be the non-linear effective diffusion (concentration dependent diffusion coefficient) as discussed in the literature.

The results indicated the following key findings: (a) mass exchange across the heterogeneity interface was not constant and it strongly changed with the hydrodynamic conditions; higher injection rate led to larger mass exchange rate, (b) mass exchange rate coefficient during loading was larger than that under unloading for the same dynamic conditions, (c) there should be a nonlinearity between the advection and diffusion (e.g., concentration-dependent diffusion) which is responsible for the larger time-scale of the unloading concentration

profiles, (d) the concentration-dependent counter-current advection-diffusion fluxes lead to slow-down periods, which are visible only during the unloading process.

Data Availability Statement

Raw data were generated at the IMPRES micromodel laboratory. Derived data supporting the findings of this study are available from the corresponding author (VN) on request.

Acknowledgments
The authors would like to acknowledge the UK Engineering and Physical Sciences Research Council (EPSRC) for funding the MITRA project (EP/R021627/1) awarded to Vahid Niasar. Hamidreza Erfani would like to acknowledge the University of Manchester for providing his PhD funding through President's Doctoral Scholarship (PDS) award. Nikolaos Karadimitriou would like to acknowledge the Deutsche Forschungsgemeinschaft (DFG, German Research Foundation) for supporting this work by funding SFB 1313, Project Number 327154368. I. Zarikos would like to thank NWO for the project Fundamental Fluid Dynamics Challenges in Inkjet Printing (FIP), i43.

References

Ahkami, M., Roesgen, T., Saar, M. O., & Kong, X.-Z. (2019). High-resolution temporo-ensemble PIV to resolve pore-scale flow in 3D-printed fractured porous media. *Transport in Porous Media*, *129*(2), 467–483. https://doi.org/10.1007/s11242-018-1174-3

Alajmi, A., Grader, A., & Alkafeef, S. (2009). Evaluation of tracer diffusion in layered system using X-ray CT. *Petroleum Science and Technology*, *27*(11), 1134–1150. https://doi.org/10.1080/15567030902929132

Alfaro, M. C., & Wong, R. C. (2001). Laboratory studies on fracturing of low-permeability soils. *Canadian Geotechnical Journal*, *38*(2), 303–315. https://doi.org/10.1139/t00-096

An, S., Hasan, S., Erfani, H., Babaei, M., & Niasar, V. (2020). Unravelling effects of the pore-size correlation length on the two-phase flow and solute transport properties: GPU-based pore-network modeling. *Water Resources Research*, *56*(8), e2020WR027403. https://doi.org/10.1029/2020wr027403

Aziz, R., Joekar-Niasar, V., & Martinez-Ferrer, P. (2018). Pore-scale insights into transport and mixing in steady-state two-phase flow in porous media. *International Journal of Multiphase Flow*, *109*, 51–62

Babadagli, T. (2003). Evaluation of EOR methods for heavy-oil recovery in naturally fractured reservoirs. *Journal of Petroleum Science and Engineering*, *37*(1–2), 25–37. https://doi.org/10.1016/s0920-4105(02)00309-1

Bear, J. (2013). *Dynamics of fluids in porous media*. Courier Corporation.

Beavers, G. S., & Joseph, D. D. (1967). Boundary conditions at a naturally permeable wall. *Journal of Fluid Mechanics*, *30*(1), 197–207. https://doi.org/10.1017/s0022112067001375

Berkowitz, B. (2002). Characterizing flow and transport in fractured geological media: A review. *Advances in Water Resources*, *25*(8–12), 861–884. https://doi.org/10.1016/s0309-1708(02)00042-8

Berkowitz, B., Cortis, A., Dentz, M., & Scher, H. (2006). Modeling non-fickian transport in geological formations as a continuous time random walk. *Reviews of Geophysics*, *44*(2). https://doi.org/10.1029/2005rg000178

Berkowitz, B., & Scher, H. (2009). Exploring the nature of non-fickian transport in laboratory experiments. *Advances in Water Resources*, *32*(5), 750–755. https://doi.org/10.1016/j.advwatres.2008.05.004

Bodin, J., Delay, F., & De Marsily, G. (2003). Solute transport in a single fracture with negligible matrix permeability: 1. Fundamental mechanisms. *Hydrogeology Journal*, *11*(4), 418–433. https://doi.org/10.1007/s10040-003-0268-2

Boon, M., Bijeljic, B., & Krevor, S. (2017). Observations of the impact of rock heterogeneity on solute spreading and mixing. *Water Resources Research*, *53*(6), 4624–4642. https://doi.org/10.1002/2016wr019912

Bromly, M., & Hinz, C. (2004). Non-fickian transport in homogeneous unsaturated repacked sand. *Water Resources Research*, *40*(7). https://doi.org/10.1029/2003wr002579

Carey, A. E., Wheatcraft, S. W., Glass, R. J., & O'Rourke, J. P. (1995). Non-fickian ionic diffusion across high-concentration gradients. *Water Resources Research*, *31*(9), 2213–2218. https://doi.org/10.1029/95wr01679

Chen, Y., Steeb, H., Erfani, H., Karadimitriou, N. K., Walczak, M. S., Ruf, M., et al. (2021). Nonuniqueness of hydrodynamic dispersion revealed using fast 4d synchrotron x-ray imaging. *Science Advances*, *7*(52), eabj0960. https://doi.org/10.1126/sciadv.abj0960

Chen, Z., Ma, X., Zhan, H., Dou, Z., Wang, J., Zhou, Z., & Peng, C. (2022). Experimental investigation of solute transport across transition interface of porous media under reversible flow directions. *Ecotoxicology and Environmental Safety*, *238*, 113566. https://doi.org/10.1016/j.ecoenv.2022.113566

Cortis, A., Gallo, C., Scher, H., & Berkowitz, B. (2004). Numerical simulation of non-Fickian transport in geological formations with multiple-scale heterogeneities. *Water Resources Researc*h, *40*(4). https://doi.org/10.1029/2003wr002750

Dejam, M., Hassanzadeh, H., & Chen, Z. (2014). Shear dispersion in a fracture with porous walls. *Advances in Water Resources*, *74*, 14–25. https://doi.org/10.1016/j.advwatres.2014.08.005

De Smedt, F., & Wierenga, P. (1979). Mass transfer in porous media with immobile water. *Journal of Hydrology*, *41*(1–2), 59–67. https://doi.org/10.1016/0022-1694(79)90105-7

De Vries, E. T., Raoof, A., & Van Genuchten, M. T. (2017). Multiscale modelling of dual-porosity porous media; a computational pore-scale study for flow and solute transport. *Advances in Water Resources*, *105*, 82–95.

De Windt, L., Cabrera, J., & Boisson, J. (1999). Radioactive waste containment in indurated shales: Comparison between the chemical containment properties of matrix and fractures. *Geological Society, London, Special Publications*, *157*(1), 167–181. https://doi.org/10.1144/gsl.sp.1999.157.01.13

Di Donato, G., & Blunt, M. J. (2004). Streamline-based dual-porosity simulation of reactive transport and flow in fractured reservoirs. *Water Resources Research*, *40*(4). https://doi.org/10.1029/2003wr002772

Douglas, J., Jr., & Arbogast, T. (1990). *Dual porosity models for flow in naturally fractured reservoirs* (pp. 177–221). Dynamics of Fluids in Hierarchical Porous Media.

Dunlop, P., & Stokes, R. (1951). The diffusion coefficients of sodium and potassium iodides in aqueous solution at 25. *Journal of the American Chemical Society*, *73*(11), 5456–5457. https://doi.org/10.1021/ja01155a520

Edery, Y., Geiger, S., & Berkowitz, B. (2016). Structural controls on anomalous transport in fractured porous rock. *Water Resources Research*, *52*(7), 5634–5643. https://doi.org/10.1002/2016wr018942

Erfani, H., Karadimitriou, N., Nissan, A., Walczak, M. S., An, S., Berkowitz, B., & Niasar, V. (2021). Process-dependent solute transport in porous media. *Transport in Porous Media*, *140*, 421–435. https://doi.org/10.1007/s11242-021-01655-6

Falta, R. W., & Wang, W. (2017). A semi-analytical method for simulating matrix diffusion in numerical transport models. *Journal of Contaminant Hydrology*, *197*, 39–49.

Ghassemzadeh, J., Xu, L., Tsotsis, T. T., & Sahimi, M. (2000). Statistical mechanics and molecular simulation of adsorption in microporous materials: Pillared clays and carbon molecular sieve membranes. *The Journal of Physical Chemistry B*, *104*(16), 3892–3905. https://doi.org/10.1021/jp993602h

Haddad, A. S., Hassanzadeh, H., & Abedi, J. (2012). Advective–diffusive mass transfer in fractured porous media with variable rock matrix block size. *Journal of Contaminant Hydrology*, *133*, 94–107.

Haggerty, R., Harvey, C. F., Freiherr von Schwerin, C., & Meigs, L. C. (2004). What controls the apparent timescale of solute mass transfer in aquifers and soils? A comparison of experimental results. *Water Resources Research*, *40*(1).

Haggerty, R., McKenna, S. A., & Meigs, L. C. (2000). On the late-time behavior of tracer test breakthrough curves. *Water Resources Research*, *36*(12), 3467–3479. https://doi.org/10.1029/2000wr900214

Harned, H. S., & Nuttall, R. L. (1949). The differential diffusion coefficient of potassium chloride in aqueous solutions. *Journal of the American Chemical Society*, *71*(4), 1460–1463. https://doi.org/10.1021/ja01172a090

Hasan, S., Joekar-Niasar, V., Karadimitriou, N. K., & Sahimi, M. (2019). Saturation dependence of non-fickian transport in porous media. *Water Resources Research*, *55*(2), 1153–1166. https://doi.org/10.1029/2018WR023554

Hasan, S., Niasar, V., Karadimitriou, N. K., Godinho, J. R. A., Vo, N. T., An, S., et al. (2020). Direct characterization of solute transport in unsaturated porous media using fast x-ray synchrotron microtomography. *Proceedings of the National Academy of Sciences*, *117*(38), 23443–23449. https://doi.org/10.1073/pnas.2011716117

Houseworth, J., Asahina, D., & Birkholzer, J. (2013). An analytical model for solute transport through a water-saturated single fracture and permeable rock matrix. *Water Resources Research*, *49*(10), 6317–6338. https://doi.org/10.1002/wrcr.20497

Jamet, D., Chandesris, M., & Goyeau, B. (2009). On the equivalence of the discontinuous one-and two-domain approaches for the modeling of transport phenomena at a fluid/porous interface. *Transport in Porous Media*, *78*(3), 403–418. https://doi.org/10.1007/s11242-008-9314-9

Karadimitriou, N., & Hassanizadeh, S. (2012). A review of micromodels and their use in two-phase flow studies. *Vadose Zone Journal*, *11*(3). https://doi.org/10.2136/vzj2011.0072

Karadimitriou, N., Joekar-Niasar, V., Hassanizadeh, S., Kleingeld, P., & Pyrak-Nolte, L. (2012). A novel deep reactive ion etched (DRIE) glass micro-model for two-phase flow experiments. *Lab on a Chip*, *12*(18), 3413–3418. https://doi.org/10.1039/c2lc40530j

Karadimitriou, N. K. (2013). *Two-phase flow experimental studies in micro-models* (Unpublished doctoral dissertation). UU Department of Earth Sciences.

Karadimitriou, N. K., Joekar-Niasar, V., Babaei, M., & Shore, C. A. (2016). Critical role of the immobile zone in non-fickian two-phase transport: A new paradigm. *Environmental Science and Technology*, *50*(8), 4384–4392. https://doi.org/10.1021/acs.est.5b05947

Layton, W. J., Schieweck, F., & Yotov, I. (2002). Coupling fluid flow with porous media flow. *SIAM Journal on Numerical Analysis*, *40*(6), 2195–2218. https://doi.org/10.1137/s0036142901392766

Le Borgne, T., & Gouze, P. (2008). Non-fickian dispersion in porous media: 2. Model validation from measurements at different scales. *Water Resources Research*, *44*(6). https://doi.org/10.1029/2007wr006279

Lima, R., Ishikawa, T., Imai, Y., Takeda, M., Wada, S., & Yamaguchi, T. (2008). Radial dispersion of red blood cells in blood flowing through glass capillaries: The role of hematocrit and geometry. *Journal of Biomechanics*, *41*(10), 2188–2196. https://doi.org/10.1016/j.jbiomech.2008.04.033

Ling, B., Oostrom, M., Tartakovsky, A. M., & Battiato, I. (2018). Hydrodynamic dispersion in thin channels with micro-structured porous walls. *Physics of Fluids*, *30*(7), 076601. https://doi.org/10.1063/1.5031776

Ling, B., Tartakovsky, A. M., & Battiato, I. (2016). Dispersion controlled by permeable surfaces: Surface properties and scaling. *Journal of Fluid Mechanics*, *801*, 13–42. https://doi.org/10.1017/jfm.2016.431

Maloszewski, P., Büttner, G., Apel, G., Krafft, H., Scholz, M., & Wagner, B. (2005). Quantitative evaluation of tracer experiments in alpine karst and porous aquifers in the national park of Berchtesgaden. *Landschaftsökologie und Umweltforschung*, *48*, 11–18.

Masciopinto, C. (2006). Simulation of coastal groundwater remediation: The case of nardò fractured aquifer in southern Italy. *Environmental Modelling and Software*, *21*(1), 85–97. https://doi.org/10.1016/j.envsoft.2004.09.028

Matuura, R., & Koga, Y. (1959). Self-diffusion of iodide ion and strontium ion in strontium iodide solutions. *Bulletin of the Chemical Society of Japan*, *32*(10), 1143–1148. https://doi.org/10.1246/bcsj.32.1143

McCall, D. W., & Douglass, D. C. (1965). The effect of ions on the self-diffusion of water. 1. Concentration dependence. *The Journal of Physical Chemistry*, *69*(6), 2001–2011. https://doi.org/10.1021/j100890a034

Moreno, L., & Tsang, C. F. (1991). Multiple-peak response to tracer injection tests in single fractures: A numerical study. *Water Resources Research*, *27*(8), 2143–2150. https://doi.org/10.1029/91wr00507

Mosthaf, K., Baber, K., Flemisch, B., Helmig, R., Leijnse, A., Rybak, I., & Wohlmuth, B. (2011). A coupling concept for two-phase compositional porous-medium and single-phase compositional free flow. *Water Resources Research*, *47*(10). https://doi.org/10.1029/2011wr010685

Murphy, H. D., Tester, J. W., Grigsby, C. O., & Potter, R. M. (1981). Energy extraction from fractured geothermal reservoirs in low-permeability crystalline rock. *Journal of Geophysical Research*, *86*(B8), 7145–7158. https://doi.org/10.1029/jb086ib08p07145

Mutch, R. D., Scott, J. I., & Wilson, D. J. (1993). Cleanup of fractured rock aquifers: Implications of matrix diffusion. *Environmental Monitoring and Assessment*, *24*(1), 45–70. https://doi.org/10.1007/bf00568799

Ochoa-Tapia, J. A., & Whitaker, S. (1995). Momentum transfer at the boundary between a porous medium and a homogeneous fluid—I. Theoretical development. *International Journal of Heat and Mass Transfer*, *38*(14), 2635–2646. https://doi.org/10.1016/0017-9310(94)00346-w

Ohlsson, Y., & Neretnieks, I. (1995). *Literature survey of matrix diffusion theory and of experiments and data including natural analogues* (Tech. Rep.). Swedish Nuclear Fuel and Waste Management Co.

Padilla, I. Y., Yeh, T.-C. J., & Conklin, M. H. (1999). The effect of water content on solute transport in unsaturated porous media. *Water Resources Research*, *35*(11), 3303–3313. https://doi.org/10.1029/1999wr900171

Paradis, D., Ballard, J.-M., Lefebvre, R., & Savard, M. M. (2018). Multi-scale nitrate transport in a sandstone aquifer system under intensive agriculture. *Hydrogeology Journal*, *26*(2), 511–531.

Polak, A., Grader, A. S., Wallach, R., & Nativ, R. (2003). Chemical diffusion between a fracture and the surrounding matrix: Measurement by computed tomography and modeling. *Water Resources Research*, *39*(4). https://doi.org/10.1029/2001wr000813

Roubinet, D., De Dreuzy, J.-R., & Tartakovsky, D. M. (2012). Semi-analytical solutions for solute transport and exchange in fractured porous media. *Water Resources Research*, *48*(1). https://doi.org/10.1029/2011wr011168

Roubinet, D., De Dreuzy, J.-R., & Tartakovsky, D. M. (2013). Particle-tracking simulations of anomalous transport in hierarchically fractured rocks. *Computers & Geosciences*, *50*, 52–58. https://doi.org/10.1016/j.cageo.2012.07.032

Saffman, P. G. (1971). On the boundary condition at the surface of a porous medium. *Studies in Applied Mathematics*, *50*(2), 93–101. https://doi.org/10.1002/sapm197150293

Shaik, A. R., Rahman, S. S., Tran, N. H., & Tran, T. (2011). Numerical simulation of fluid-rock coupling heat transfer in naturally fractured geothermal system. *Applied Thermal Engineering*, *31*(10), 1600–1606. https://doi.org/10.1016/j.applthermaleng.2011.01.038

Sharma, P. K., Shukla, S. K., & Pran, S. (2016). Experimental and numerical modeling of solute transport through fractured sedimentary rock mass. *ISH Journal of Hydraulic Engineering*, *22*(3), 274–280. https://doi.org/10.1080/09715010.2016.1201781

Shaw, S., Ganguly, S., Sibanda, P., & Chakraborty, S. (2014). Dispersion characteristics of blood during nanoparticle assisted drug delivery process through a permeable microvessel. *Microvascular Research*, *92*, 25–33. https://doi.org/10.1016/j.mvr.2013.12.007

Siegrist, R. L., Lowe, K. S., Murdoch, L. C., Case, T. L., & Pickering, D. A. (1999). In situ oxidation by fracture emplaced reactive solids. *Journal of Environmental Engineering*, *125*(5), 429–440. https://doi.org/10.1061/(asce)0733-9372(1999)125:5(429)

Siirila-Woodburn, E. R., Sanchez-Vila, X., & Fernàndez-Garcia, D. (2015). On the formation of multiple local peaks in breakthrough curves. *Water Resources Research*, *51*(4), 2128–2152. https://doi.org/10.1002/2014wr016394

Sudicky, E., & Frind, E. (1982). Contaminant transport in fractured porous media: Analytical solutions for a system of parallel fractures. *Water Resources Research*, *18*(6), 1634–1642. https://doi.org/10.1029/wr018i006p01634

Suzuki, A., Fomin, S., Chugunov, V., & Hashida, T. (2018). Mathematical modeling of non-fickian diffusional mass exchange of radioactive contaminants in geological disposal formations. *Water*, *10*(2), 123. https://doi.org/10.3390/w10020123

Tang, D., Frind, E., & Sudicky, E. A. (1981). Contaminant transport in fractured porous media: Analytical solution for a single fracture. *Water Resources Research*, *17*(3), 555–564. https://doi.org/10.1029/wr017i003p00555

Wan, J., Tokunaga, T. K., Tsang, C.-F., & Bodvarsson, G. S. (1996). Improved glass micromodel methods for studies of flow and transport in fractured porous media. *Water Resources Research*, *32*(7), 1955–1964. https://doi.org/10.1029/96wr00755

Wang, L., Stuart, M., Lewis, M., Ward, R., Skirvin, D., Naden, P., et al. (2016). The changing trend in nitrate concentrations in major aquifers due to historical nitrate loading from agricultural land across England and wales from 1925 to 2150. *Science of The Total Environment*, *542*, 694–705. https://doi.org/10.1016/j.scitotenv.2015.10.127

Wang, P. P., Zheng, C., & Gorelick, S. M. (2005). A general approach to advective–dispersive transport with multirate mass transfer. *Advances in Water Resources*, *28*(1), 33–42.

Weishaupt, K., Joekar-Niasar, V., & Helmig, R. (2019). An efficient coupling of free flow and porous media flow using the pore-network modeling approach. *Journal of Computational Physics X*, *1*, 100011. https://doi.org/10.1016/j.jcpx.2019.100011

West, M. R., Kueper, B. H., & Novakowski, K. S. (2004). Semi-analytical solutions for solute transport in fractured porous media using a strip source of finite width. *Advances in Water Resources*, *27*(11), 1045–1059. https://doi.org/10.1016/j.advwatres.2004.08.011

Wu, M., Xiao, F., Johnson-Paben, R. M., Retterer, S. T., Yin, X., & Neeves, K. B. (2012). Single-and two-phase flow in microfluidic porous media analogs based on Voronoi tessellation. *Lab on a Chip*, *12*(2), 253–261. https://doi.org/10.1039/c1lc20838a

Zhu, W., Liu, J., Elsworth, D., Polak, A., Grader, A., Sheng, J., & Liu, J. (2007). Tracer transport in a fractured chalk: X-Ray CT characterization and digital-image-based (DIB) simulation. *Transport in Porous Media*, *70*(1), 25–42.